International Journal of Environment, Agriculture and Biotechnology
Vol-8, Issue-5; Sep-Oct, 2023
Peer-Reviewed International Journal
Journal Home Page Available: https://ijeab.com/
Journal DOI: 10.22161/ijeab

Analysis of Urban Thermal Environment Effect by TIRS and GIS: A Case Study of Zhuhai, Guangdong

Tingjun Zhang[1], Ruei-Yuan Wang*[2], Zhe Zhu[3], Yun-Shang Wang[4]

[1,2,3]School of Sciences, Guangdong University of Petrochem Technology(GDUPT), Maoming 525000, China
[4]Graduate Institute, Fu Jen Catholic University
Corresponding author*

Received: 16 Aug 2023; Received in revised form: 21 Sep 2023; Accepted: 04 Oct 2023; Available online: 13 Oct 2023

Abstract— *The rapid development of urbanization in China is not only reflected in the tight land area and rapid population growth but also causes changes in the local urban climate, such as the increasingly obvious urban heat island effect (UHIE). This study explores the impact of urban surface cover types on the urban thermal environment. Taking Zhuhai City, Guangdong Province as an example, based on Landsat-8 thermal infrared remote sensing (TIRS) data, the atmospheric correction method (also known as Radiation Transfer Equation, RTE) and spilt-window inversion algorithm are used to invert the land surface temperature (LST) of the study area and compare their accuracy. After applying ArcGIS to normalize the data, the standard deviation method was used to classify the LST and obtain the distribution map of surface temperature levels in the urban area. In addition, the urban heat island proportion index was used to evaluate the UHIE in the study area, and the distribution of UHIE intensity was obtained. Based on geographical and national data, a combination of mathematical and spatial statistics was used to establish a correlation between the proportion of underlying surface coverage and LST in three different types of water bodies: vegetation and impermeable water surfaces. The results of the effect of urban underlying surface layout on the thermal environment were obtained, and the overall thermal environment effect of the city was obtained.*

Keywords— ***Thermal Infrared Sensor (TIRS); Land Surface Temperature (LST); Radiative Transfer Equation (RTE); Underlying Surface; Urban Heat Island Effect (UHIE).***

I. INTRODUCTION

Land surface temperature (LST) is of great research significance in the fields of urban thermal environment changes, landscape pattern analysis, and ecological characteristics' analysis, and is an important parameter for studying the exchange of matter and energy between land and atmosphere. In recent years, scholars have conducted research on LST based on remote sensing (RS) technology (Price, 1990; Yue et al., 2006), ranging from LST inversion to results analysis and application. One of the hotspots is the quantitative analysis of the relationship between urban surface temperature changes and the underlying surface (which is an important factor in climate formation and refers to the Earth's surface interacting with the atmosphere during heat, momentum, and water vapor exchange).

For example, Atsuko et al. (2009) pointed out after studying the impact of land use and land cover (LULC) on ambient temperature in Takamatsu City, Japan, that the growth of urban impermeable underlying surface area is one of the most important factors leading to temperature rise. Xiao et al. (2007) further found that there is a positive correlation between the impermeable underlying surface and LST in Beijing. Streutker (2002) and Roth et al. (1989) used RS data to invert LST and its spatial distribution in several cities along the western coast of North America. They believe that there is a clear correlation between the thermal characteristics inside cities during the day and land use, while the correlation between nighttime heat island intensity and land use is relatively small. Chen et al. (2006) and Li et al. (2008) analyzed the correlation between NDVI (Normalized Difference Vegetation Index), MNDWI (Modified Normalized Difference Water Index), NDBI (Normalized Difference Building Index), and NDBSI (Normalized Difference Bare Soil Index) and LST, respectively. They found a clear correlation between them, and there were significant differences in LST among different LULC types. The above study obtained the correlation between underlying surface and temperature in different types of cities.

This article takes Zhuhai City, Guangdong Province, as an example and uses Landsat-8 thermal infrared (band) image data as the basis to invert its LST. Combined with the geographical and national data of the research area, a quantitative analysis is conducted on the relationship between surface temperature and underlying surface in order to provide scientific reference for the evaluation of natural resource ecological environment and urban planning in domestic cities.

II. STUDY AREA AND DATA SOURCE

2.1 Study Area

Zhuhai City has three administrative regions under its jurisdiction: Xiangzhou, Doumen, and Jinwan. The location is superior, bordering the South China Sea, with a distance of 36 nautical miles from Hong Kong's waterway to the east and connected to Macau's land to the south. After the completion of the Hong Kong-Zhuhai-Macau Bridge, Zhuhai has become the only city on mainland China that is connected to both Hong Kong and Macau by land. Zhuhai is an important port city in China, with five land transportation ports, including Gongbei, Hengqin, Qingmao, the Hong Kong- Zhuhai-Macao Bridge, the Zhuhai Highway, and the Zhuhai-Macao Cross-Border Industrial Zone. There are 5 water transportation ports, including Jiuzhou Port, Wanzai Port for ferry passenger transportation, Zhuhai Port, Doumen Port, and Wanshan Port. There are a total of 10 national first-class ports, making it the second-largest port city in China after Shenzhen. It has rich marine resources, vast sea areas, and numerous islands.

The climate of Zhuhai is pleasant, with an obvious alternation of winter and summer winds. The temperature is relatively high all year, with occasional cold showers. The annual and daily temperature differences are small, and they belong to the transitional marine climate between the South Asian tropics and the tropics. The city is rich in solar energy and abundant in heat. It is the only city in China that has been selected as one of the "Top 40 National Tourist Attractions" for its overall urban landscape, with mountains and rivers alternating and land islands facing each other (Figure 1 and Figure 2).

with land use status maps.

(4) The climate pattern of Guangdong Province has been characterized by a continuous increase in temperature since June, with a high temperature period from July to September and a significant UHIE. Therefore, when selecting data sources, priority should be given to image data from June to September. However, due to the large amount of cloud cover in the image data during this time span, it will have a serious impact on temperature inversion. Thus, after further evaluation, February images were selected for inversion analysis.

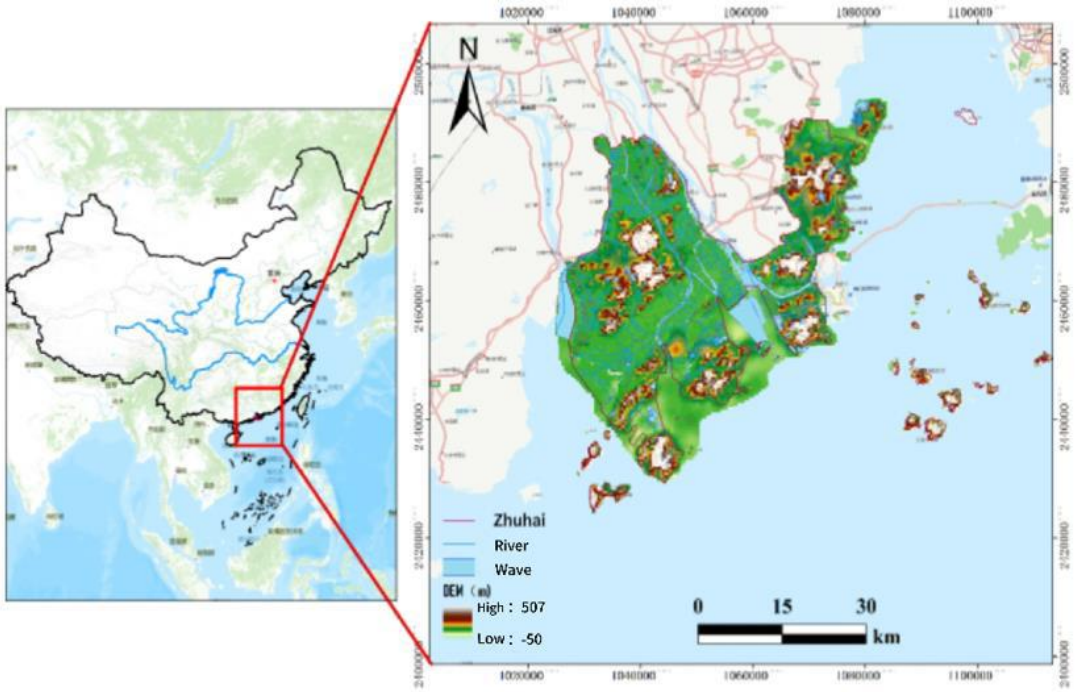

Fig.1 Geographical Area Map of Zhuhai City

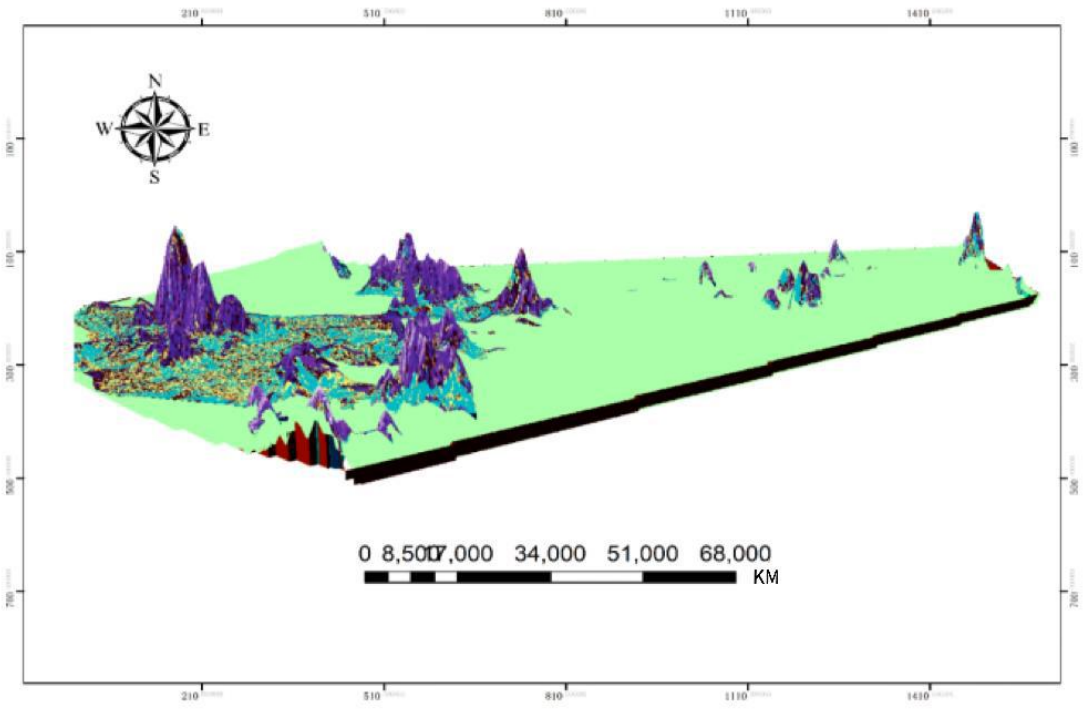

Fig.2 Topographic Profile of Zhuhai

2.2 Data Source and Preprocessing

The data sources used in this study chiefly include geographic national condition vectors and Landsat-8 satellite images.

(1) Geographic national vector data includes surface coverage data from the 2017 Geographic National Survey and the 2020 Geographic National Monitoring results.

(2) Landsat-8 satellite images, including three thermal infrared image data from February 7, 2016, February 17, 2016, and February 20, 2021.

(3) To compare the different temperature changes of the underlying surface in Zhuhai in different years, two

images were selected for analysis and comparison. When selecting images from the source database, it was found that the number of available images was relatively small. Thus, an image mosaic method was adopted to obtain the full image of February 2016. Among them, the 10th and 11th bands of the Landsat-8 thermal infrared sensor (TIRS) are used to estimate brightness temperature; the operational land imager (OLI) data is used to calculate the NDVI, MNDWI, and NDBI. Next, the data is subjected to radiometric calibration processing and FLAAS atmospheric correction. In addition, land use types are based on NDVI, MNDWI, and NDBI, using normalized density segmentation methods for classification, and calibrated in conjunction

III. METHODOLOGY

This study selected Zhuhai City as the research area, comprehensively utilizing various methods such as geographic information systems (GIS), RS technology, and spatial modeling. Based on multi-temporal Landsat image data, a supervised classification method is used to classify land use/cover. The RTE method and split-window algorithm are used to invert LST in order to study the characteristics of underlying surface changes and the spatio-temporal changes of LST during urbanization. Analysis of the relationship between underlying surface changes and LST uses the quantitative method. The specific research route is as follows (Figure 3):

(1) Analysis of the spatio-temporal dynamics of underlying surface changes: Using land use/cover change (LUCC) as the characteristic, the spatio-temporal dynamics of underlying surface changes are analyzed, as well as the characteristics of landscape pattern changes in Zhuhai's underlying surface from the perspective of patch types and landscape levels.

(2) Analysis of spatio-temporal characteristics of LST changes based on RS inversion data in Zhuhai City from 2016 to 2021. And using methods such as urban heat island proportion index analysis, normalize the retrieved temperature for hierarchical classification, analyze the spatial agglomeration effect of LST, and explore the differences in the contribution of land use/cover types in different regions and underlying surfaces to the urban thermal environment.

(3) Analysis of the relationship between the underlying surface and surface temperature based on statistical methods to clarify the characteristics of LST changes on the underlying surface and explore the relationship between changes in the underlying surface and LST.

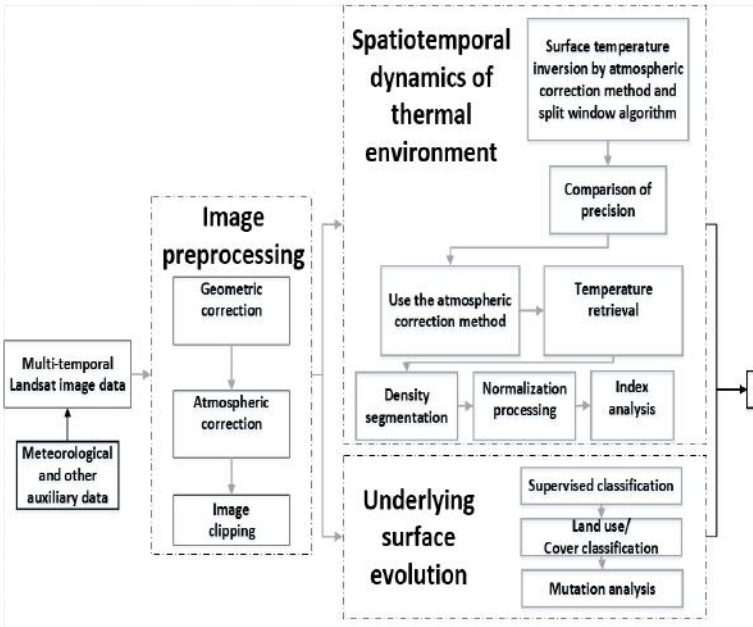

Fig.3 the Schema Flowchart of the Study

3.1 LST Inversion

3.1.1 Radiative Transfer Equation (RTE) Method

■Basic principle:

There are three main types of LST inversion based on RS: the RTE, the single channel algorithm, and the split-window algorithm. Among them, retrieving LST requires three parameters, namely: average atmospheric temperature, atmospheric transmittance, and surface emissivity.

The main approach is to first estimate the impact of the atmosphere on surface thermal radiation, and then subtract the atmospheric impact from the total amount of thermal radiation observed by satellite sensors to obtain the intensity of surface thermal radiation, and then convert the intensity of thermal radiation into the corresponding surface temperature.

■Basic steps:

1. Data Preprocessing

(1) Calculate radiation brightness temperature (T6): After radiation correction and atmospheric correction are

applied to the multispectral and thermal infrared bands, calculate radiation brightness temperature (b1 selects the thermal infrared band after radiation correction).

T6=k2/ln (k1/B (TS)+1) (1)

In the formula (1), B (TS) is the thermal radiation brightness of the blackbody in TS derived from Planck's law, and T is the transmittance of the atmosphere in the thermal infrared band. The radiation brightness B (TS) of a blackbody at temperature T in the thermal infrared band is as formula (2):

$$B(TS) = [L\lambda - L\uparrow - \tau\cdot(1-\varepsilon)L\downarrow]/(\tau\cdot\varepsilon) \quad (2)$$

λ is the thermal radiation brightness of the blackbody at TS, which is derived from Planck's law.

k2=1321.08, k1=774.89 are preset constants for Landsat-8 band10 before transmission, and after substitution, formula (3) is obtained.

T6=1321.08/log (774.89/b1+1) (3)

(2) NDVI calculation such as formula (4): b3 and b4, respectively, select the red and near-infrared bands after atmospheric correction.

NDVI= (float (b4 b3))/(b4+b3) (4)

(3) Vegetation coverage FVC calculation: NDVIS and NDVIV generally use the minimum edge value of the vegetation index and the maximum vegetation index. This article uses a 5% confidence interval, and the calculation formula is as follows (formula 5):

FVC= (NDVI - NDVIS)/(NDVIV NDVIS)
= (b1 gt 0.506826) * 1+(b1 lt 0.156625) * 0+(b1 ge 0.156625 and b1 le 0.506826) * (b1-0.156625)/(0.506826-0.156625)) (5)

(4) Surface emissivity (Surf) is a basic parameter of LST that mainly depends on the geological structure of the surface. This study uses the same surface emissivity calculation method as TM/ETM+6. Calculate surface emissivity using the NDVI threshold method proposed by Sobrino (2006). In band math, the formula is converted to:

Surf=0.004 * b1+0.986 (6)

In the formula, b1 is vegetation coverage (VFC)

2. LST Inversion

(1) Calculate variables C and D, as shown in formulas (7) and (8):

C = 0.34 * b1 (7)

D= (1-t) * (1+(1-b1) * t) (8)

(b1 represents the surface emissivity (Surf), 0.34 is the atmospheric transmittance of the day; the atmospheric transmittance is obtained by inputting the photography time and central latitude and longitude through NASA's official website.)

(2) Calculate the surface temperature in degrees Celsius using the formulas (9), (10), and (11):

Ts=[a * (1-C-D)+(b * (1-C-D)+C+D) * T6+D * Ta]/C (9)

(Ts is the true surface temperature; a and b are constants; a = -67.355351, b = 0.458606.) C and D are intermediate variables, as shown in formulas (7) and (8). The radiant brightness temperature T6 can be obtained using the inverse function of the Planck formula (as shown in formula 3), where Ta is the average atmospheric temperature (in K). In addition, there is a linear relationship between the average atmospheric temperature Ta and the near surface temperature T0 (usually 2m) as follows:

Ta=17.9769+0.91715 * T0 (tropical average atmosphere)

Ta=16.0110+0.92621 * T0 (mid-latitude summer average atmosphere)

Ta=19.2704+0.91118 * T0 (mid-latitude winter average atmosphere)

Among them, Ta is the average atmospheric temperature, and T0 is the local temperature at the time of remote sensing image acquisition (T0's temperature needs to be converted into Kelvin temperature).

Ta=17.97669+0.91715 * (273.15+19)=285.992 (10)

LST=Ts-273.15 (11)

In the above equation, the conversion formula between Kelvin (K) and Celsius (℃) is: K=℃+273.15, ℃=K -273.15. Among them, K represents Kelvin, and ℃

represents Celsius. Thus, subtracting 273.15 from Kelvin K is the value of degrees Celsius.

3.1.2 Double-Channel Nonlinear Split-Window Algorithm

(1) LST Inversion Algorithm

Using the dual channel nonlinear split-window algorithm to invert surface temperature (Chen et al., 2004) (as shown in formula 12):

$$T = b_0 + \left(b_1 + b_2\frac{1-\varepsilon}{\delta} + b_3\frac{\Delta\varepsilon}{\delta^2}\right)\frac{T_i+T_j}{2} + \left(b_4 + b_5\frac{1-\varepsilon}{\delta} + b_4\frac{\Delta\varepsilon}{\delta^2}\right)\frac{T_I-T_J}{2} + b_7(T_I - T_J)^2 \quad (12)$$

Among them, e and Δε Represent the mean and difference of emissivity for two channels, depending on surface classification and coverage: T_I and T_J are the observed brightness temperatures of two channels, b_i (i=0, 1... 7) represents various coefficients that can be obtained from simulated datasets of laboratory data, atmospheric parameter data, and atmospheric radiation transfer equations. To improve inversion accuracy, coefficient b_i depends on the water vapor content in the atmospheric column.

(2) Atmospheric Water Vapor Content

To reduce dependence on external atmospheric conditions, a new algorithm has been developed to estimate water vapor from thermal infrared images themselves. Firstly, an empirical relationship between the atmospheric transmittance ratio T_i/T_J of two split window channels and the atmospheric water vapor content wv is established using MODTRAN and TIGR atmospheric profiles. Then, the transmittance ratio is estimated using the ratio of covariance to variance between the brightness temperatures of the two channels within a certain size sliding window (as shown in formula 13)..

$$wv = a + b\left(\frac{T_I}{T_J}\right) + c.(T_I/T_J)^2 \quad (13)$$

(3) Pixel Emissivity Inversion

The vegetation coverage weighting method uses Landsat-8 visible and near-infrared data to invert NDVI and vegetation coverage f to estimate pixel emissivity.

$$\varepsilon_p = \varepsilon_v.f + \varepsilon_g(1-f) + 4 < d\varepsilon > f.(1-f) \quad (14)$$

f= (NDVI-NDVIs)/ NDVIv-NDVIs)^2 (15)

Among them, the emissivity data of vegetation components ε and the emissivity data of background components ε_g come from the spectral database. The <dε> represents the cavity effect parameter formed by multiple scattering of components within a pixel, which is determined by the red structure of the pixel canopy and surface roughness. NDVIs and NDVIv are NDVI values for bare soil and dense vegetation, respectively. To maintain consistency between different images of NDVIs and NDVIv, fixed values are taken here, namely NDVIs=0.2 and NDViv=0.86. When the NDVI of a pixel is greater than NDVIv, the plate coverage of the pixel is 10, and the emissivity of the pixel is ε_v. When the NDVI of a pixel is less than NDVIs, the vegetation cover of the pixel is 0,0; Pixel reflectance is ε_g .

3.2 Quantitative Analysis of LST Change and Underlying Surface

This study is based on the results of surface coverage in geographical and national conditions. Within the study area, quantitative analysis is conducted on the relationship between LST changes and underlying surfaces, including the urban heat island proportion index and the analysis of the relationship between underlying surfaces and LST changes. Among them, the urban heat island proportion index is a new viewpoint proposed to address the difficulty of quantitative comparison of UHIE in different time periods. That is, the comparison of UHIE between different time periods cannot only consider the temperature itself but also the different temperature levels that make up the urban heat island, the proportion of the area in the urban built-up area (Li, 2020), and the contribution of temperature intensity to the formation of the heat island effect to analyze the urban heat island proportion index (Sun, 2020).

The analysis of urban heat island proportion index is based on the inversion of LST, obtaining information such as the highest temperature, lowest temperature, and average temperature in the study area, and analyzing the spatial distribution characteristics of LST in each study area. And density classification technology is used to classify, calculate, and analyze the absolute value of LST. In addition, analysis of the relationship between underlying surface and LST changes: analyze the LST of

the study area in 2016 and 2021, and calculate the area and proportion of LST at all levels; Based on geographical and national land cover data, calculate the area and proportion of different types of underlying surfaces within different levels of temperature; Based on statistical results, quantitatively analyze the relationship between LST changes and underlying surfaces.

IV. ANALYSIS AND RESULTS

The underlying surfaces of this study are divided into three categories: vegetation, water bodies, and impermeable surfaces, where impermeable surfaces refer to surfaces covered by various impermeable building materials, such as buildings, roads, and parking lots composed of materials such as tiles, asphalt, cement concrete, etc.

4.1 Vegetation Information Extraction

The most commonly used vegetation information extraction is the normalized difference vegetation index (NDVI), which is between -1 and 1. The vegetation index is positive, and the larger the value, the more obvious the vegetation features. The calculation formula is shown in (11), and the vegetation cover map is shown in Figure 4:

$$NDVI=\frac{NIR-RED}{NIR+RED} \quad (11)$$

where RED and NIR, respectively, select the red and near-infrared bands after atmospheric correction.

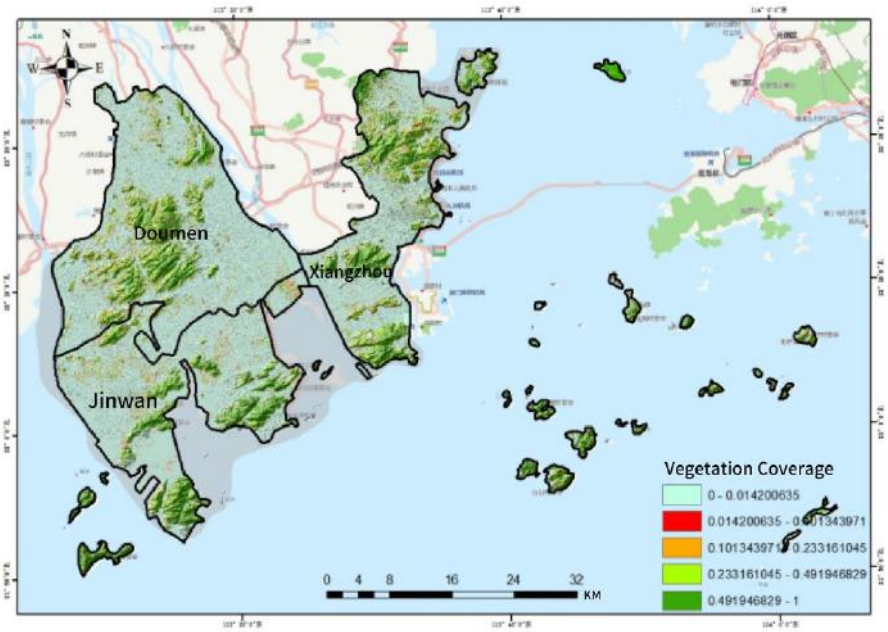

Fig.4 Vegetation Cover Map of Zhuhai City

4.2 Water Body Information Extraction

Mcfeeters (Vitousek, et al., 2008) proposed the Normalized Difference Water Index, abbreviated as the NDWI. Its formula is as follows (12):

$$NDWI=\frac{BGreen-BNIR}{BGreen+BNIR} \quad (12)$$

where BGreen represents the green light band; BNIR represents the near-infrared band.

The basic principle of the model is that as the reflection of water gradually weakens from visible light to the mid-infrared wavelength range, it has the strongest absorption in the near-infrared and mid-infrared wavelength ranges and almost no reflection. Therefore, the NDWI composed of the contrast between the visible and near-infrared bands can highlight the water body information in the image (the NDWI value of the water body is the largest). In addition, due to the generally strongest reflectance of vegetation in the near-infrared band, the ratio of the green light band to the near-infrared band can be used to suppress vegetation information to the greatest extent, thereby achieving the goal of highlighting water information (Figure 5).

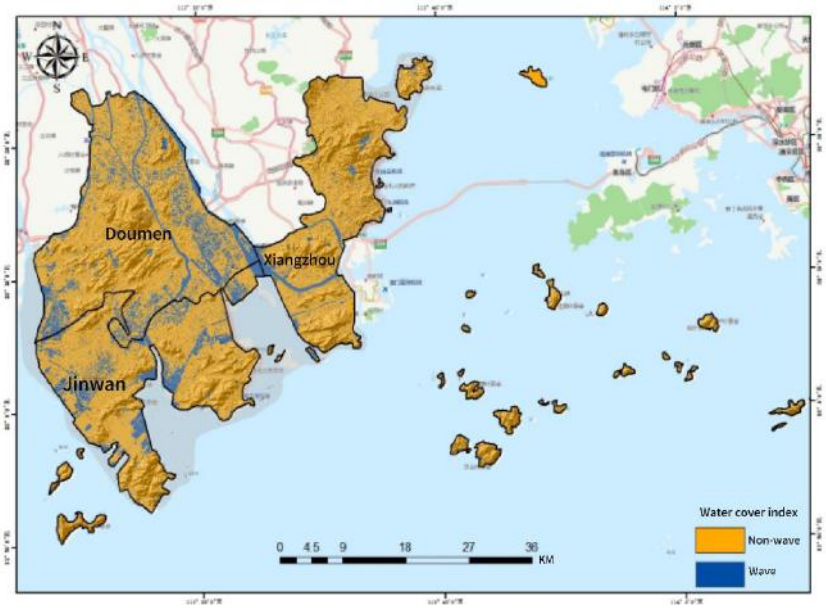

Fig.5 Water Cover Map of Zhuhai City

4.3 Urban Construction Land Information Extraction

NDBI is proposed based on the pseudo-normalized difference vegetation index proposed by Yang (Zhuang et al., 2019). It can accurately reflect information about building land. A larger value indicates a higher proportion of building land and a higher building density. Through visual interpretation, the NDBI threshold is continuously adjusted until a suitable threshold is found, and construction land is extracted. After adjusting the threshold, the impermeable water surface distribution is obtained. The calculation formula is as follows (13):

$$\text{NDBI}=\frac{RMIR-\text{BNIR}}{BMIR+\text{BNIR}} \quad (13)$$

where RNIR and RMIR are the reflected radiation values of the near-infrared and mid-infrared images, corresponding to the band 5 and band 6 OLI data. The darker the color of the NDBI image, the higher the representative value, indicating a higher proportion of building land and a higher density of buildings (Figure 6).

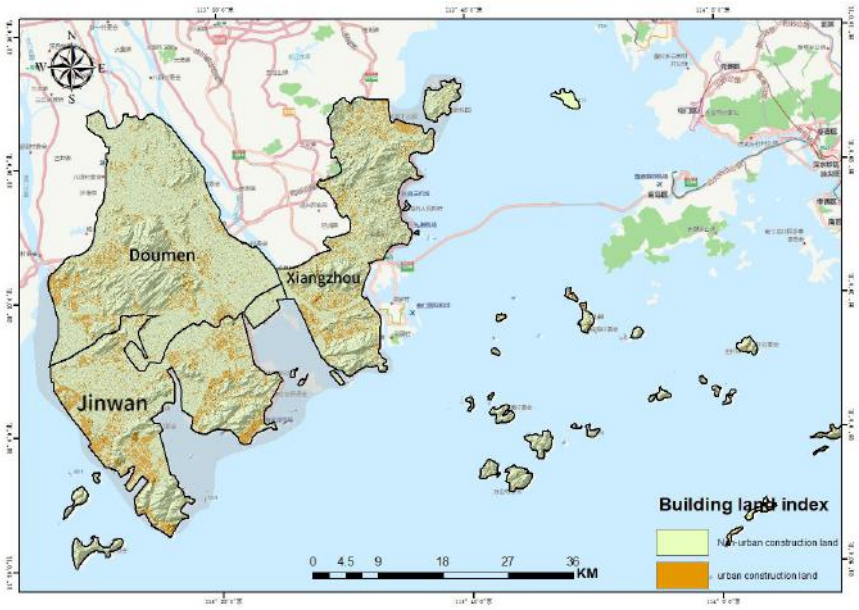

Fig.6 Construction Land Coverage Map of Zhuhai City

4.4 Analysis of UHI Ratio Index

The proportion of vegetation area in the urban area of Zhuhai remained unchanged from 2016 to 2021, while the proportion of water body area decreased slightly and the proportion of impermeable water surface area increased. According to the geographical and national survey and monitoring data statistics of Guangdong Province (Figure 7 and Table 1).

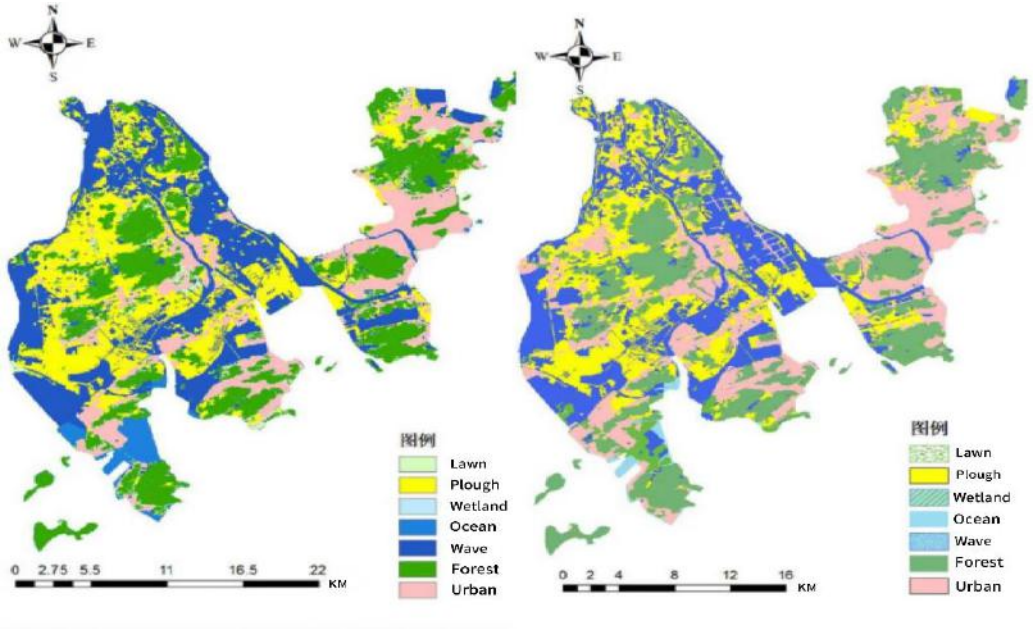

Fig.7 Remote Sensing Images of Land Use in Zhuhai in 2016 and 2021

(Image Source: 2022 GlobeLand30 Surface Cover Data from the Ministry of Natural Resources of China)

Table 1 Proportion of Different Underlying Surface Areas in Zhuhai in 2016 and 2021

Study area	Category	Year of 2016		Year of 2021	
		Area /km^2	Ratio （%）	Area /km2	Ratio （%）
Zhuhai City District	Water bodies	468.84	27	416.75	24
	Vegetation	573.03	33	573.03	33
	Impervious surface	260.47	15	382.02	22

4.5 Inverted LST Situation

The surface temperature situation of Landsat-8 remote sensing image data for temperature inversion is shown in Figure 8 and Table 2. The atmospheric correction method, also known as the RTE method, is based on the Planck equation to invert surface temperature. This method is simple and clear and has higher inversion accuracy when obtaining or simulating more accurate atmospheric parameters. Compared with the dual-channel nonlinear split-window algorithm, it reduces the impact of atmospheric water vapor content on temperature data with a smaller standard deviation. The data is relatively stable and the error is small, so this article uses the atmospheric correction method for the temperature inversion of Zhuhai City in relevant years.

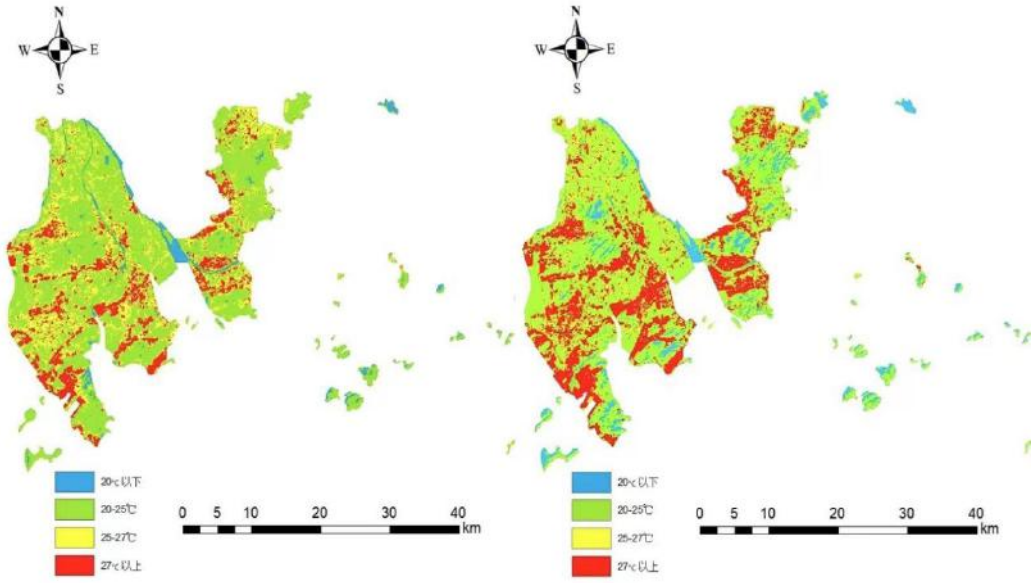

Fig.8 Temperature Inversion Image in 2021
[Split Window Algorithm (Left), Atmospheric Correction Method (Right)]

Table 2 Statistical Characteristics of Temperature Inversion

Study area	Method	Highest	Minimum	Average temperature	Standard deviation
Zhuhai	Split-window	42.499	10.958	24.174	2.411
	RTE	37.777	11.407	22.222	1.884

The surface temperature situation of the reverse performance (Figure 9, Table 3) shows that the daily highest and lowest temperatures in the urban area of Zhuhai in 2021 were higher than those in the same month of 2016. The standard deviation of temperature decreased, indicating a smaller dispersion of temperature distribution and gradually stabilizing.

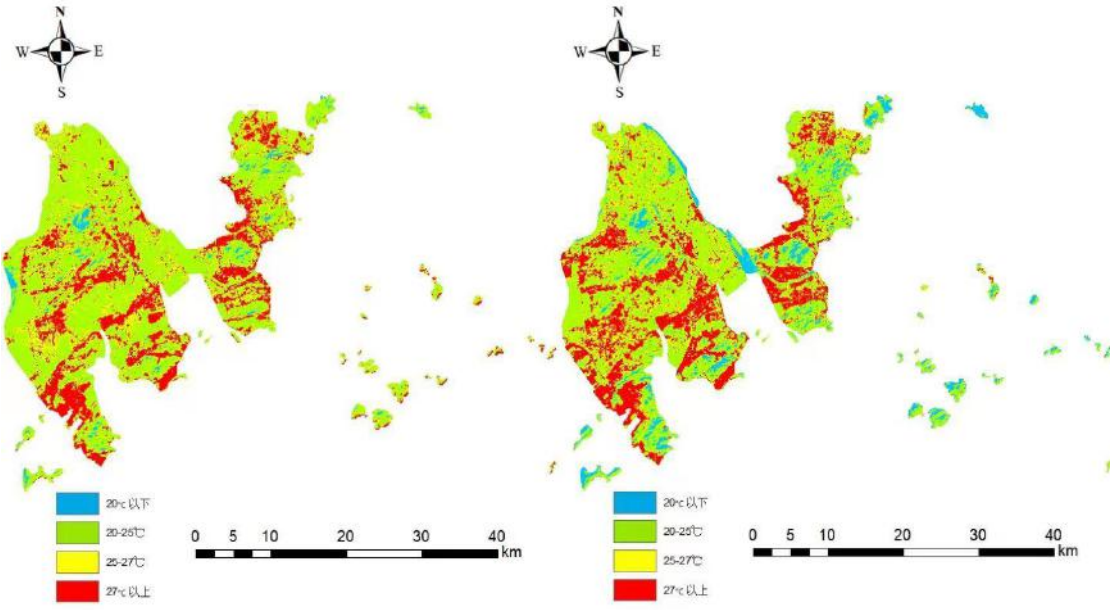

Fig.9 Temperature Inversion Image [2016 (Left) and 2021 (Right)]

Table 3 Statistical Characteristics of Surface Temperature in Zhuhai in 2016 and 2021

Study area	year	Highest	Minimum	Average temperature	Standard deviation
Zhuhai	2016	35.256	8.109	17.096	2.144
	2021	37.777	11.407	22.222	1.884

Due to the significant differences in surface temperatures among different time periods, it is not feasible to directly compare the surface temperatures of each time period. Thus, normalization and density segmentation techniques are used to classify the surface temperatures over two time periods. By calculating the urban heat island ratio index, the trend of surface temperature changes in different regions and different time periods is studied.

The specific steps are as follows: first, normalize the inverted LST according to formula (14), and unify the surface temperature between 0 and 1. Then, using density segmentation technology, the normalized s LST is divided into seven levels using an even distribution method, including extremely high temperature (EHT), high temperature (HT), relatively high temperature (RHT), medium temperature (MT), relatively low temperature (RLT), low temperature (LT), and extremely low temperature (ELT), with corresponding level values ranging from 7 to 1 (Pan and Han, 2011; Li and Xv, 2014). Finally, calculate the proportion of these levels in the built-up area and calculate the URI based on the formula (15).

$$LST_{norm}=\frac{LST-LSTmin}{LSTmax-LSTmin} \qquad (14)$$

$$URI=\frac{1}{100m}\sum_{i=1}^{n} wipi \qquad (15)$$

In the formula (14), LSTnorm is the normalized surface temperature value; LST that has not been normalized; and LSTmax is the maximum value of surface temperature. LSTmin is the minimum value of surface temperature;

In the formula (15), URI refers to the proportion of urban heat islands; m is the number of surface temperature levels; i is the temperature level in the urban area that is higher than the moderate temperature zone; n is the number of temperature levels in urban areas that are higher than those in moderate-temperature areas; W is the weight value, selecting the level value of the i-th level; and P is the percentage of level i. In this study, the natural breakpoint classification method was used to classify the LST into 7 levels, so m is 7. Areas above moderate temperatures represent the development range of urban heat islands; therefore, n is 3.

Based on the above method, the calculated values and distribution maps of Table 4 and Figure 10 were obtained. Analysis shows that in 2016, the temperate zone in the urban area of Zhuhai accounted for the largest proportion of the total area (23.6%). The sub-high temperature zone (46%) accounted for the largest proportion of the total area in 2021, with the URI increasing from 0.307 in 2016 to 0.393. Compared with 2016, the total proportion of EHT, HT, and RHT areas increased by 10.804%, resulting in an increase of 0.086 in the urban heat island proportion index of Zhuhai City. From 2016 to 2021, the surface of the urban area showed an increase in temperature, with a small increase in the range of EHT, HT, and RHT.

Table 4 Heat Island Ratio Index and Area Proportion of Temperature Class

Study area	Year	Proportion of area occupied by temperature zones, Pi/(%)							
		EHT	HT	RHT	MT	RLT	LT	ELT	URI
Zhuhai	2016	0.111	0.175	0.233	0.236	0.146	0.079	0.019	0.307
	2021	0.189	0.2	0.46	0.396	0.07	0.004	0.001	0.393

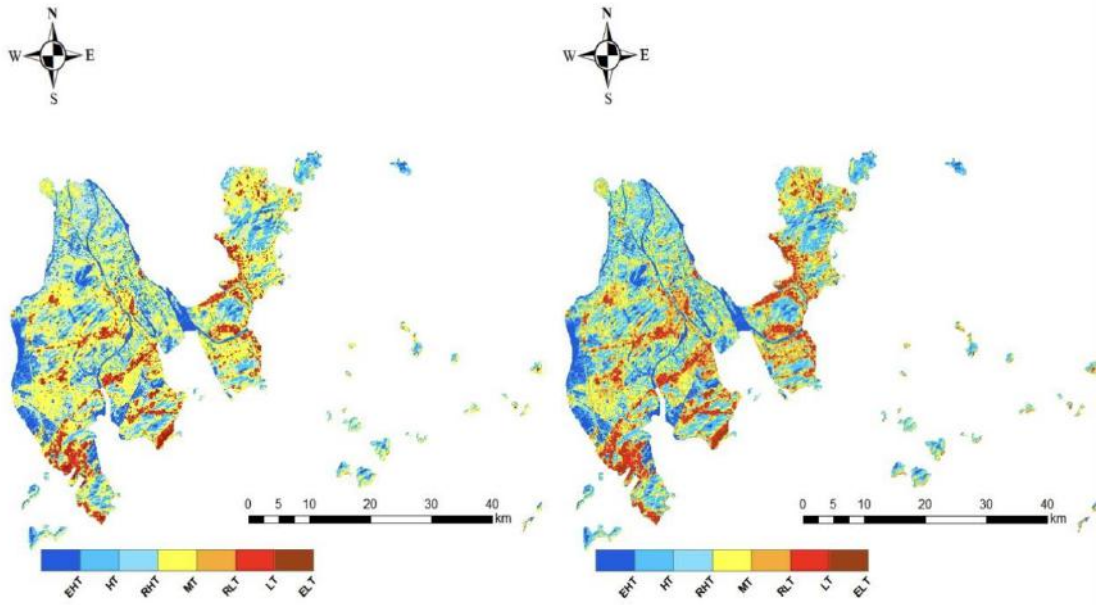

Fig.10 Temperature Inversion Normalization Processing Images
[2016 (Left) and 2021 (Right)]

4.6 Analysis of Underlying Surface and LST Change

From the perspective of underlying surfaces, compared to 2021, the proportion of underlying surfaces and impermeable surfaces in extremely high-temperature and high-temperature areas in Zhuhai City remained relatively stable at over 95% in 2016. This indicates that the high-temperature areas of the city are mainly concentrated in buildings, highways, railways, and other impermeable areas without vegetation or water cover. From 2016 to 2021, the proportion of impermeable surfaces in urban areas increased by 7%, while the proportion of water bodies decreased by 3%, with little change in the proportion of vegetation.

V. CONCLUSIONS

The study analysis shows that from 2016 to 2021, the proportion of impermeable water surface in the urban area of Zhuhai City has slightly increased, the proportion of water body area has slightly decreased, and the vegetation area remains unchanged. After careful comparison and analysis of the proportion of underlying surface area, it was found that the vegetation area on the underlying surface of Zhuhai City remained relatively stable at 33%. The proportion of water body area is about 30% (27% in 2016 and 24% in 2021). From this, it can be concluded that for small and medium-sized cities, vegetation plays a greater role in alleviating the UHIE than water bodies. That is, for small and medium-sized cities, in the process of urban development, if the high proportion of vegetation coverage in the area can be maintained, even if the proportion of impervious surface area decreases and human activity areas increase (15% in 2016 and 22% in 2021), it may not lead to a sharp intensification of the urban heat island phenomenon.

In this study, only two images of February were selected for the inversion of urban temperature. Although the months studied do not belong to the annual high temperature period, the patterns show that there are changes (increases) in urban temperature between years. However, the temperature changes throughout the year cannot be fully demonstrated, so it is insufficient to highlight the trend of heat island changes in the city. In the future, we plan to make full use of geographical and national data, refine the underlying land types, and conduct quantitative analysis of the relationship between LST changes and underlying surfaces in the study area during the four seasons in order to provide a useful reference for urban development planning.

Technically, this article uses the traditional atmospheric correction (RTE) method for LST inversion,

which has room for improvement in accuracy. In the future, we plan to optimize the inverse algorithm from the perspectives of physical simulation and mathematical statistical analysis and then compare the accuracy differences with traditional calculation results. In addition, it is not possible to verify the inversion results of surface temperature due to the lack of synchronous meteorological observation data on satellite transit time and surface temperature, and the estimation of emissivity has not addressed the issue of pixel mixing. In summary, the above analysis elements are the focus of further experiments and discussions in this study in order to improve the reliability and accuracy of LST inversion.

ACKNOWLEDGEMENTS

The author is grateful for the research grants given to Ruei-Yuan Wang from GDUPT Talents Recruitment (No.2019rc098) in Guangdong Province, China, and Academic Affairs in GDUPT for Goal Problem-Oriented Teaching Innovation and Practice Project Grant No.701-234660.

REFERENCES

[1] Atsuko, N., Mutsuko, K., Takuro, M. Impact of land use and land cover changes on the ambient temperature in a middle scale city, Takamatsu, in Southwest Japan. Journal of Environmental Management, 2009, 90 (11)：3297-3304. https://doi.org/10.1016/j.jenvman.2009.05.004

[2] Chen, X., Zhao, H., Li, P. and Yin, Z. Remote sensing image-based analysis of the relationship between urban heat island and land use/cover changes. Remote Sensing of Environment, 2006, 104(2): 133-146. https://doi.org/10.1016/j.rse.2005.11.016

[3] Chen, Y. H., Li, J., and Li, X. B. Pattern, process, simulation and influence of remote sensing analysis of urban spatial thermal environment. Beijing: Science Press, 2004.01.

[4] Li, H., Zeng, Y. N., and Liu, Q. H. A Remote Sensing Image-Based Study of The Relationship Between Urban Heat Island and Land Use/Cover Changes in Changsha City. Remote Sensing for Land & Resources, 2008, 28(4):47-52.DOI:10.3724/SP.J.1047.2008.00128.

[5] Li, L., and Xv, H. Q. Urban Expansion and Thermal Environment Changes in Hangzhou City of East China. Remote Sensing Technology & Application, 2014, 29(2).DOI:10.11873j.issn.1004-0323.2014.2.0264.

[6] Li, T. Study on the response of surface thermal environment to urban spatial structure in Beijing. Shandong Normal University, 2020,TU984.113. DOI:10.27280/d.cnki.gsdsu.2020.000934.

[7] Pan, J. H., and Han, W. C. Urban expansion and its heat island response in Lanzhou City based on remote sensing analysis. Chinese Journal of Ecology, 2011, 30(11):2597-2603.DOI:10.1007/s12583-011-0162-0.

[8] Price, J.C. Using Spatial Context in Satellite Data to Infer Regional Scale Evapotranspiration. IEEE Transactions on Geoscience and Remote Sensing，1990 ,28(5):940 -948.

[9] Roth, M, Oke, T. R.，and Emery, W. J. Satellite derived urban heat islands from three coastal cities and the utilization of such data in urban climatology. International Journal of Remote Sensing，1989，10 (11): 1699-1720. DOI:10.1080/01431168908904002

[10] Sobrino, J. A., Jimenez-Munoz, J. C., Zarco-Tejada, P. J, Sepulcre-Cantó, G., and Miguel. E. Land surface temperature derived from airborne hyperspectral scanner thermal infrared data. Remote Sensing of Environment, 2006, 102: 99-106.

[11] Streutker, D. R. A remote sensing study of the urban heat island of Houston, Texas. International Journal of Remote Sensing ， 2002 ， 23(13) ： 2595-2608. DOI:10.1080/01431160110115023

[12] Sun, Y. Research on the Impact of Urban Expansion on Urban Climate--Taking Wuhan as an Example[D].Hubei University of Technology,2016,TU119.4;TU984

[13] Vitousek, P.M., Mooney, H.A., Lubchenco, J., and Melillo, J.M. Human Domination of Earth's Ecosystems. In: Marzluff, J.M., et al. Urban Ecology. Springer, Boston, MA. 2008. https://doi.org/10.1007/978-0-387-73412-5_1

[14] Xiao, R., Ouyang, Z., Zheng, H., Li, W., Schienke, E. W., and Wang X. Spatial pattern of impervious surfaces and their impacts on land surface temperature in Beijing, China. Journal of Environmental Sciences，2007,19 (2): 250-256.

[15] Yue, W. Z., Xv, J. H., and Xv, L. H. An analysis on eco-environmental effect of urban land use based on remote sensing images: a case study of urban thermal environment and NDVI. Acta Ecologica Sinica, 2006, 26(5):1450-1460. DOI:10.1016/S1872-2032(06)60025-5.

[16] Zhuang, Y., and Xue, D. Q. Kuang W. Chi, W., and Pan, T. Spatial and temporal characteristics of land cover hierarchy in Hu-Bao-Hubei urban agglomeration in semi-arid region of China. Remote sensing technology and application, 2019, 34 (1):197-206. DOI:10.11873/j.issn.1004-0323.2019.1.0197.